Check for updates

Charge-Assisted Engineering of Color Centers in Diamond

Tobias Lühmann, Jan Meijer, and Sébastien Pezzagna*

Owing to its unique optical and spin properties, the nitrogen-vacancy (NV) center holds the promise of a diamond-based room-temperature scalable quantum computer, but the numerous technical and physical issues are not yet overcome, especially the poor N to NV conversion. The NV and other color centers are, however, successfully used as multitasking quantum sensors, and open new routes in quantum sensing technologies. Most recently, several breakthroughs and demonstrations were achieved, shedding a new light on the feasibility of a NV-based quantum computer. Herein, the recently developed method of charge-assisted single defect engineering is reviewed. With a controlled charging of the involved species, it modifies the diffusion or kinetics of defect formation and acts as a catalyzer of the NV creation while hindering the formation of competing and perturbing defects such as divacancies or NVH. Very high NV creation yields up to 75% are obtained and the method is suitable to other impurity-vacancy defects. Furthermore, it has positive consequences on the charge state stability and coherence time of the NV centers, which is as well discussed. Together with the possibility to nowadays deterministically implant single ions, this powerful method brings the scalability of NV qubits closer.

1. Introduction

The isolation of a single nitrogen-vacancy (NV) center in diamond in 1997[1] and the demonstration of coherent control of its associated electron spin at 300 K in 2004[2] committed the NV as a promising solid-state qubit.[3] Long coherence times[4] up to 2 ms at 300 K and fast (GHz) spin manipulation[5] were furthermore reported. With the availability of high purity diamond substrates and the development of ion implantation techniques, a diamond-based scalable quantum computer operating at room temperature could be envisaged. However, the first NV–NV entanglement was realized in 2013 only[6] and many preliminary issues were still to be overcome. Among these are the low NV creation yield of a few percent or less, the poorer

properties and short coherence times of implanted NV centers, charge state stability issues, or the need for spin manipulation and readout of individual NV centers at short scales (<30 nm). Meanwhile, owing to their properties of high sensitivity, high resolution, robustness, or optical readout, the NV and other color centers were successfully opening new paths in quantum sensing of magnetic field,[7] electric field,[8] pressure,[9] temperature,[10] nano-NMR,[11] and so on.

In 2019, quantum supremacy was demonstrated using 53 superconducting qubits cooled below 20 mK.[12] At the same time, several breakthroughs were achieved in different domains related to NV centers which, when considered all together, shed a new light on the possibility to build a scalable diamond-based quantum computer. First, on the fabrication side, the deterministic implantation of countable ions with high resolution was shown with Pr ions in YAG,[13] and can be adapted to nitrogen or other ions. In addition, very high NV creation yields up to 75% were obtained by means of Coulomb-driven defect engineering.[14] As well, it was shown that the creation and migration of vacancies can be achieved with a pulsed laser and that, when coupled to a confocal microscope, the birth of a single NV from a native nitrogen can be controlled in real time.[15] On the side of the qubits addressing, the manipulation and optical readout of the first entangled NV–NV system at 300 K (with 25 nm separation)[6] was relying on the fact that the two NVs were oriented differently and had different lifetimes, which is not scalable at all. Nowadays, the photoelectric detection of magnetic resonance (PDMR) was demonstrated on single NV centers.[16] Furthermore, it was shown that the microwave manipulation of the spin of shallow NV centers can be achieved in the near-field using transparent and conducting stripes deposited on top of them.[17,18] These two techniques get rid of optical diffraction and may enable an individual addressing and readout of individual NVs at high resolution using nanosized stripes. At 300 K, single-qubit and two-qubit gates fidelities of 99.9952% and 99.2% were demonstrated,[19] within <10 ns[5] and 700 ns.[19] This NV operation performance, together with T_2 coherence times (up to the ms range[4,20]), is comparable with superconducting qubits but at mK. Furthermore, the number of qubits and qubit connectivity can be largely increased (for the same number of connections and wires) by taking advantage of the NV hyperfine coupling to several neighboring and randomly distributed ^{13}C nuclear spins (1.1% natural abundance with respect to 98.9% of spin-free ^{12}C). This was demonstrated

T. Lühmann, Prof. J. Meijer, Dr. S. Pezzagna
Applied Quantum Systems, Felix-Bloch Institute for Solid-State Physics
Universität Leipzig
Linnéstraße 5, 04103 Leipzig, Germany
E-mail: sebastien.pezzagna@uni-leipzig.de

The ORCID identification number(s) for the author(s) of this article can be found under https://doi.org/10.1002/pssa.202000614.

at 4 K using up to 10 and even 27 ^{13}C atoms in the studies by Bradley et al.[21] and Abobeih et al.,[22] respectively, with memory times of about 75 s and two-qubit entanglement preserved for more than 10 s. Quantum computers based on solids with coherently switchable electron and nuclear spins represent therefore a promising alternative to the recently achieved quantum computer based on superconducting qubits[23] or cold ions; not only from the scalability, operation, and robustness point of view but also from the manufacturing and operating costs.[24] A way toward entanglement among the different qubits is strong coupling between adjacent electronic spin centers using dipolar magnetic interactions (which scales as distance d^{-3}). Typical cut-off distances are limited by the electron spin dephasing time and are around 30 nm for NV centers (assuming $T_2 \approx 1$ ms) in diamond at 300 K.[6]

The full scalability of defect centers in diamond and other solid-state hosts relies therefore on the ability to create on demand countable single centers with high spatial resolution. This involves, on the one hand, the deterministic implantation of single ions and, on the other hand, the activation of the implanted species into the desired active centers. The first section will give an overview of the state of the art of the different ion implantation techniques. More particularly, the fact that deterministic implantation techniques are now available justifies the need for an advanced and targeted defect engineering. The principles of this recently applied method, its efficiency, and the properties of the color centers obtained in this way will be discussed in the second part.

2. Toward Deterministic Ion Implantation with High Spatial Resolution

Color centers can be produced either by chemical vapor deposition (CVD) growth or by ion implantation, both at high density and at the single center level. However, only ion implantation offers the possibility of a 3D placement and the choice of any ion species (which may not incorporate during the growth process), but at the cost of the production of lattice defects. Ion implantation is a well-established method widely used in the semiconductor industry to modify the properties of materials (electrical, mechanical, optical, chemical, etc.). Nowadays, the standard creation of NV and other centers for application in quantum sensing or quantum information processing relies on the stochastic implantation of atoms, followed by a thermal treatment. The annealing is required to form the impurity-vacancy centers (NV, SiV, SnV, etc.) mostly through vacancy diffusion and to heal the implantation defects. In such a case, both the implantation and the impurity-vacancy formation are stochastic processes. Taking the example of an array of NV centers created by large-scale nitrogen implantation through a mask (with an array of holes produced by electron beam lithography), the distribution of the number of NV centers per hole will inevitably follow Poissonian statistics. Thus, scalability is impossible, as shown in **Figure 1**.

In Figure 1a,b, arrays of 30 nm diameter holes were prepared in poly(methyl methacrylate) (PMMA) by electron beam
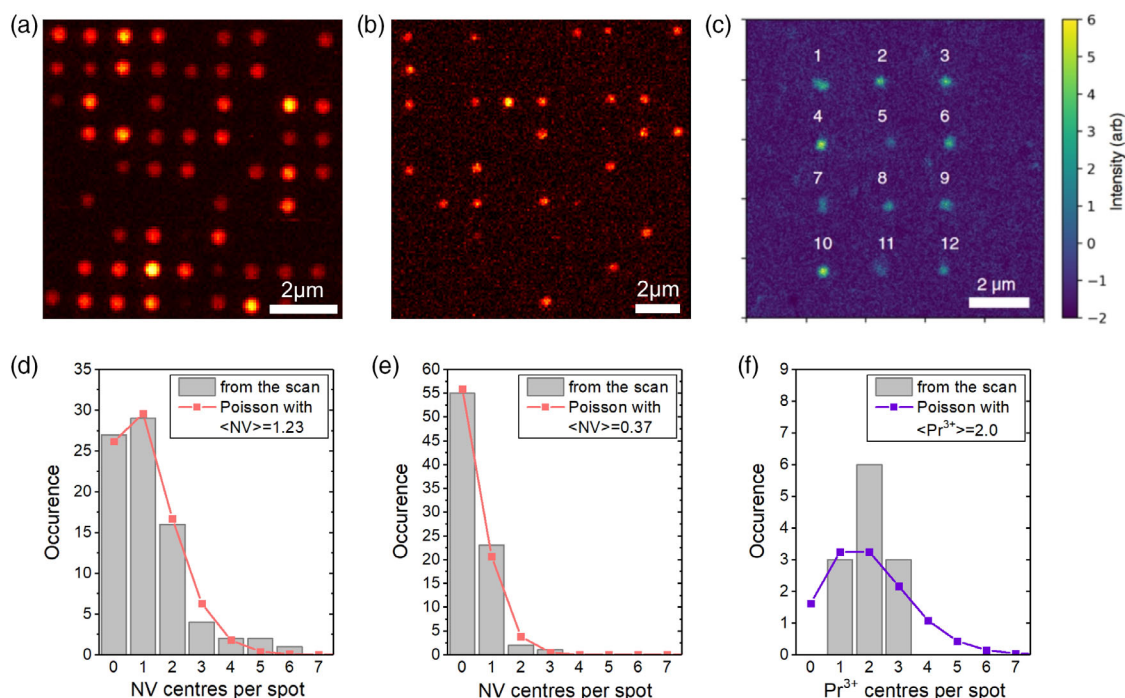

Figure 1. a,b) Confocal fluorescence scans of arrays of NV centers in diamond created by nitrogen implantation (30 keV) through a PMMA lithographic mask with 30 nm holes. The ion fluences of 3.5×10^{12} cm^{-2} and 1.4×10^{12} cm^{-2} correspond to an average of 25 and 10 nitrogen ions per spot, respectively, aiming at 1 NV center per spot in average. The sample was annealed at 900 °C in vacuum for 2 h. d,e) Occurrence of the number of NV centers per spot corresponding to (a) and (b), respectively. Poissonian distributions with a mean value of 1.23 and 0.37 are plotted. c) Array of Pr^{3+} ions in a YAG crystal created by deterministic implantation of Pr$^+$ ions (at 5.9 keV) and thermal annealing in air at 1200 °C for 1 min. Exactly four ions per spot (two ions for spot #12) were implanted. The conversion to active Pr^{3+} ions was estimated to be 50%. Reproduced with permission.[13] Copyright 2019, APS Physics. f) Occurrence of the number of Pr^{3+} ions per spot together with a Poissonian distribution with mean value of 2.0. The Pr^{3+} distribution is clearly sub-Poissonian.

lithography. Two different nitrogen fluences were implanted, corresponding to 25 and 10 nitrogen per hole, respectively, aiming at an array with on average one NV per spot (assuming a creation efficiency of 3–5% for the energy of 30 keV[25]). As expected, the fluorescence scans reveal incomplete arrays with empty places. The distribution of the number of NVs per spot is in both cases very well matched by a Poissonian distribution

$$\mathcal{P}(n) = \frac{\overline{n}^n}{n!}e^{-\overline{n}} \tag{1}$$

On the contrary, Figure 1c shows the deterministic implantation of Pr^+ ions in a YAG crystal.[13] The Pr^{3+} ions replace Y^{3+} ions in the YAG lattice and can be imaged with a confocal microscope doing upconversion of photons in the UV.[26] Here, exactly four Pr ions were implanted at each location using a directly focused beam (without any mask). The YAG sample was then annealed to remove the implantation defects and a creation yield of 50% was found. The distribution of the number of Pr^{3+} centers per spot reveals a sub-Poissonian statistics, different from the NV centers. Assuming the deterministic implantation of individual ions in an array containing n sites, the probability to obtain the full array of n active qubits (with each qubit produced with a yield Y) scales like $(Y)^n$. Therefore, the aim of the methods discussed in Section 4 is to render the N to NV (and other impurity-vacancy) formation as high as possible and eventually deterministic as well.

2.1. High-Resolution Ion Implantation

The depth of implanted ion species is well defined and controlled at the nm level by the ion kinetic energy. Ion straggling and ion channeling, however, introduce uncertainties in the depth positioning, which increase with the ion energy.[27] These two physical processes are well understood and impose a limit on the implantation energy to ensure nanometer longitudinal precision. Typically, this is achieved using energies <10 keV. It is furthermore possible to avoid ion channeling by implanting with an incidence angle a few degrees off from any main crystal axis. A detailed study of the channeling effect for low energy ions is found in the study by Raatz et al.[28] Several methods were thus developed to reach high lateral resolution as well and to obtain a full 3D nm positioning. The implantation of nitrogen into diamond to form NV centers was an ideal playground. The brightness and stability of single NV centers make them easy to image with standard confocal microscopy. In addition, NVs are also an ideal system for subdiffraction imaging like stimulated emission depletion (STED) microscopy, down to a few nm of lateral resolution,[29] i.e., comparable with the ion spread to be measured. Among these methods, implantation through a pierced AFM tip,[30,31] using photoresist masks,[32,33] nanotracks in mica[6,34] or by direct nitrogen-FIB writing[35] enabled to reach lateral resolution of <15, 30, <40, and <90 nm, respectively. The shallow implantation of NVs using a SEM is an alternative method producing very shallow NVs with good optical and spin properties.[36] For some applications, the implantation of N_2 molecules can as well provide very small distance between the two nitrogen atoms, or the use of larger molecules such as

adenine may enable a genuine defect engineering.[37] However, all these methods provide only an average number of ions estimated from the ion current and implantation time.

2.2. Deterministic Ion Implantation Methods

The full color center scalability requires a deterministic implantation of countable ions. The different methods already tested and relying on pre- or postimpact detection are presented here.

2.2.1. Secondary Electrons

The method is based on the detection of the secondary electrons produced by the impact of a single ion (**Figure 2**a).[38] To obtain a stream of individual ions, the ion beam is collimated by a small aperture and chopped at high frequency. This one-by-one deterministic method was demonstrated by the implantation, within the channel of a field-effect transistor, of a controlled number of dopant atoms (P^{2+} ions at 30 kV) in an ordered array with 60 nm precision.[39]

2.2.2. Electron–Hole Pairs

The principle of this method is adapted from the ion-beam-induced charge (IBIC) technique. Here, the collection of electron–hole pairs created by the impact of a single ion in the substrate is used as postimpact detection. A sketch is shown in Figure 2b and more details are found in the study by Jamieson et al.[40] The target substrate must, however, enable the preparation of an integrated detection system and the detection of low energy ions <10 keV is challenging.

2.2.3. Cold Ions in a Paul Trap

This technique delivers single countable ions (in the energy range 0.5–30 keV) with high resolution for any target substrate. The source consists in an ion trap, loaded with laser cooled $^{40}Ca^+$ ions[41] and sympathetically cooled $^{141}Pr^+$ ions (Figure 2e). The fluorescence of the Ca ions is imaged on a camera, which enables to count the number of trapped ions, to reveal the presence of dark ions, and to determine their mass by a weighting process. A voltage sequence applied on the axial trap potential reduces the number to exactly one Ca^+ and one Pr^+. The ions are then extracted and focused to the target with a beam waist of about 30 nm for Pr. This was demonstrated by the creation of Pr^{3+} centers in a YAG crystal, as shown in Figure 1c.[13] The positioning accuracy may be improved to a few nm by improving the cooling and the mechanical and thermal stability of the system. Other ion species and especially nitrogen could also be loaded into the trap.

2.2.4. Heralded Rydberg Atoms

A proof of principle demonstration of a high repetition deterministic single ion source was reported by Sahin et al.[42] The source consists of a magnetooptical trap where rubidium atoms are photoionized (Figure 2c). The creation of an ion is heralded by the
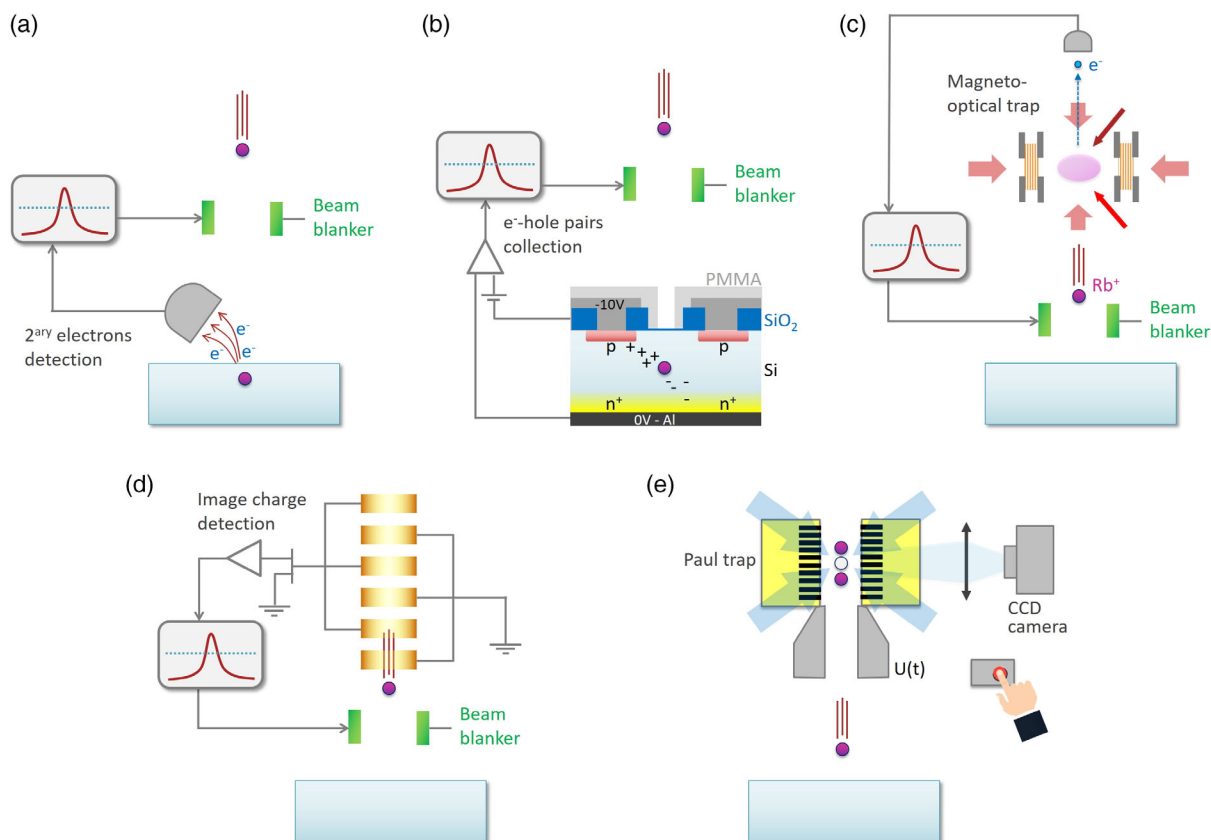
Figure 2. Techniques for deterministic ion implantation. a) Detection of secondary electrons.[38] b) Detection of electron–hole pairs.[40] c) Rydberg atoms heralded by electron detection.[42] d) Image charge detection.[43] e) Paul trap with sympathetically cooled ions.[13]

corresponding electron. The timing information of the electron is used to manipulate the trajectory of the ion in flight. The technique is, however, limited to atomic species which can be laser cooled.

2.2.5. Image Charge Detection

This method is based on the detection of an ion passing through conductive rings, as shown in Figure 2d,[43] which induces a moving image charge, i.e., a current signal. Although not yet able to detect a single charge, it is universal and versatile. If an ion is detected, the beam blanking is switched off and the ion will be implanted. In any other case, the ion is not implanted. The advantage is to never produce false-negative implantations. The serial arrangement of many rings allows producing a measurable periodic signal with a well-defined frequency (because the ion velocity is well known). To achieve single charge detection, technical challenges such as the low signal to noise (very low current despite very sensitive electronics) or the limited bandwidth by the length of the detector need still to be overcome. Fast and low-noise electronics must be used; about 2 µs are allowed for decision-making (beam deflection on or off) after detection. The method is still under development but promising results were already achieved.[44]

3. Impurity-Vacancy Defect Formation

3.1. Creation Yield of NV Centers: The Old Problem

The first artificial creation of NV centers in diamond using direct nitrogen implantation was achieved in 2005[45] using a tandem accelerator which produces MeV ions penetrating deep inside the material and giving relatively high NV creation yield. Nevertheless, for the two most foreseen applications of NV centers, a much lower energy of a few keV or less is required. On the one hand, NV magnetometry relies on the magnetic dipolar interaction between the NV electron spin and the external spins or magnetic domains. These interaction scales like the distance at the third power and it is therefore necessary to have shallow NV centers close to the diamond surface to obtain the highest sensitivity and imaging resolution. On the other hand, quantum information processing applications require the very exact placement of the different NV qubits in the nm range. This can only be ensured by low implantation energies ≤ 10 keV. It was, however, shown that the NV creation yield possesses a strong ion energy dependence,[25] with extremely low values of a few percent or less in the energy range of interest below 10 keV. **Figure 3**c is a plot of the number of nitrogen required to obtain one NV center in average, in the standard annealing conditions (800–900 °C in vacuum for a few hours). The reasons for this are multiple: 1) The
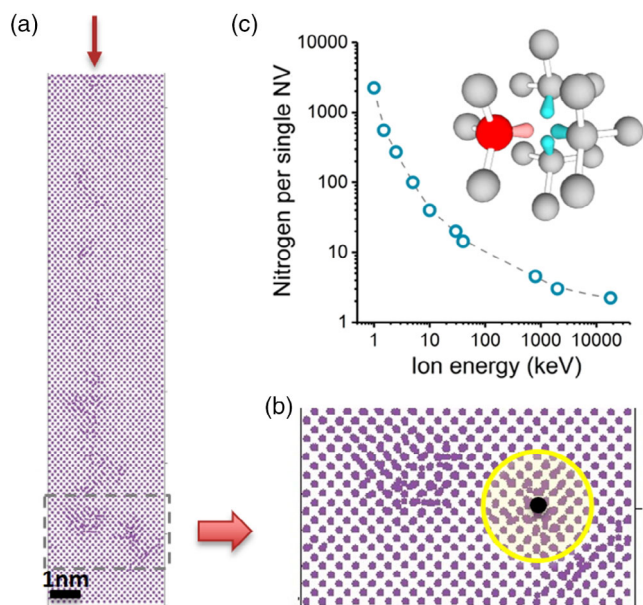
Figure 3. a) Molecular dynamics simulation of a 4 keV nitrogen atom implanted into a (001) diamond. Reproduced with permission.[47] Copyright 2018, IOP Science. b) Zoom at the end of range where the ion stops. About five to seven vacancies are found within a 1 nm diameter volume around the nitrogen ion. c) Number of nitrogen needed to be implanted to create one NV center, as a function of the nitrogen ion energy, for standard annealing conditions (800–900 °C in vacuum for a few hours). The inset shows the structure of the NV center.

number of vacancies produced per implanted ion diminishes when the ion energy is reduced, thus giving a lower probability to form an NV center.[25,46,47] 2) During thermal annealing, the vacancies become mobile (Section 3.4) and have a chance to reach the diamond surface and to be lost, especially in the case of the very low energies. The vacancy diffusion is expected to be larger close to the diamond surface.[48] 3) The diamond–air interface induces a band bending which can lead to a depth-dependent charge state occupation of the defects during annealing and of the created NV centers.[49] 4) The vacancies likely build complexes especially divacancies and even voids,[14,46,47,50] which are extremely stable[51] and consume them instead of being available to form NV centers. Moreover, molecular dynamics (MD) simulations indicate that the proportion of divacancies (V_2) increases when the implantation becomes shallower.[50]

Figure 3a is a MD simulation illustrating the clustering of vacancies at low energy implantation.[47] An average of five to seven vacancies is always found around the final position of the nitrogen ion. This shows that there are enough vacancies available and at a reachable distance. However, only in 1% of the cases, this leads to the formation of one NV center. It is therefore now admitted that the formation of vacancy complexes is one of the main competitors to NV center formation, together with the interstitial–vacancy recombination.

To increase the number of impurity-vacancy centers, a postirradiation of the sample can generally be employed to create additional vacancies, and then to thermally anneal the sample after or during the irradiation. Depending on the application, on the

scale (individual centers or bulk) or on the type of targeted defects, there is the choice between electrons, protons, neutrons, gamma rays, light ions, heavy ions, or laser, which were all already used in the past. A summary of the different possibilities can be found in the study by Smith et al.[52] or Zaitsev.[53] Here, a few examples of conversion of native N to NV centers are shown in **Figure 4**, using electrons, C^+ ions,[54] Os^+ ions,[55] or pulsed laser.[15]

3.2. Other Color Centers

The small lattice constant of diamond implies low solubility of impurities, large strain, and favors the association of the impurities with other defects and especially with the lattice vacancy.[56] As seen previously, the creation yield of NV centers (by nitrogen implantation and thermal annealing) has a strong ion energy dependence and is rather low for ion energies <10 keV. Nevertheless, a low efficiency (of a few percent at best) appears to be a common feature of all impurity-vacancy centers, which indicates that the availability and diffusion of vacancies are limited by competing processes. Here, we shortly review the creation efficiency of other color centers in intrinsic diamond.

Column IV impurity-vacancy centers (SiV, GeV, SnV, and PbV) are as well intensively studied as an alternative to the NV center.[57–59] All of them could be created and observed at the single center level. They share the same defect structure of a split interstitial vacancy where the impurity atom lies between the two vacancies along a <111> direction. They have D_{3d} symmetry, contrarily to the NV center which involves one vacancy and has C_{3v} symmetry. In the ion energy range between 10 and 100 keV, the SiV^- creation yield shows only a weak increase and lies between 1% and 2.5% (with a thermal annealing at 1050 °C for 2 h in vacuum).[60] If the ion fluence exceeds 10^{12} cm^{-2}, the creation yield starts to drop. No improvement of the 1–2% yield was found between 800 and 1100 °C in the study by Evans et al.[61] A much larger value of 15% was, however, reported in the study by Tamura et al.[62] for similar conditions. As for NV centers, a higher SiV yield (tenfold) can be obtained by postcreation of vacancies; this was shown using an electron irradiation and annealing.[60]

For the GeV center, the yield is about 0.6% for 35 keV energy and 30 min at 1000 °C.[63,64] Both SiV and GeV can be obtained during CVD growth; however, the creation of SnV centers was achieved by ion implantation only.[65,66] Several peaks are generally observed in photoluminescence (PL), but only the zero-phonon line (ZPL) at 620 nm was attributed to the SnV^-. Owing to the large size of the Sn atom, higher temperatures and or pressures are required to heal the larger implantation defects. Using a high-pressure high-temperature (HPHT) treatment at 2100 °C under 7.7 GPa removes all PL lines except the 620 nm SnV$^{[65,67]}$ and gives a creation efficiency in the range 1–4% for 150 keV. Similar values were reported (for Sn at about 80 keV) at lower temperatures and no pressure applied: from 0.6% at 800 °C to 2.5% at 1200 °C, 4 h each[14] and 5% at 950 °C for 2 h.[66] It is even more challenging to produce PbV centers due to the very large Pb atom. Nevertheless, PbV could be fabricated with a 2% yield when implanted at the energy of 20 keV and annealed at 1200 °C.[68]
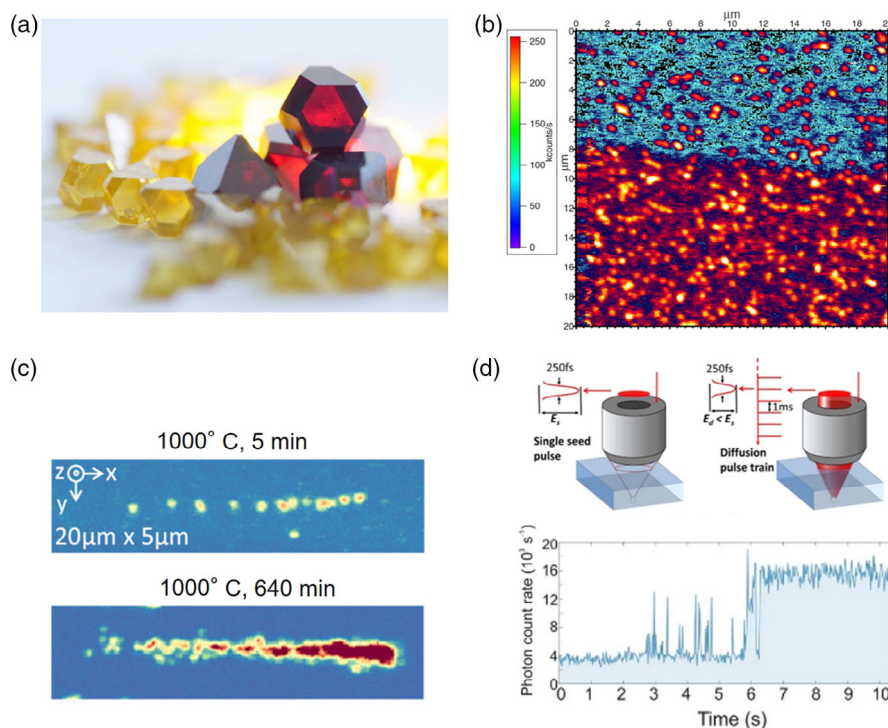
Figure 4. Postimplantation methods for NV yield enhancement. a) High energy (10 MeV) and high fluence electron irradiation of Ib HPHT yellow diamonds (0.1 and 0.3 carat, [N] ≈ 100 ppm) turn them into red diamonds ([NV] ≈ 10 ppm) after thermal annealing. b) Low energy carbon implantation (40 keV) followed by thermal annealing at 800 °C for 2 h. A IIa CVD diamond was preimplanted with NV centers. The confocal image shows the effect of the carbon implantation (lower half), revealing an increased NV density. a,b) Reproduced with permission.[54] Copyright 2010, American Institute of Physics. c) Confocal fluorescence scans of high energy (490 MeV) single Os ion tracks revealed by NV formation after thermal annealing. Each ion is expected to produce 35 000 vacancies which can convert the native nitrogen of a type IIa CVD diamond ([N] = 3–4 ppb) to NV centers. Reproduced with permission.[55] Copyright 2017, Wiley-VCH. d) Laser-induced vacancies and NV centers. The combination of a pulsed Ti:Sa laser with a confocal microscope enables the creation of vacancies, their diffusion, and the "birth" of individual NV centers which can be monitored in real time, as shown here on the fluorescence trace. Reproduced under the terms of the Creative Commons Attribution 4.0 license.[15] Copyright 2019, The Authors. Published by Optical Society of America.

Other promising centers were reported in the last years, especially the ST1 center which is, to date, the only optical center, together with the NV, showing optically detected magnetic resonance (ODMR) at room temperature.[69–71] Its nature is not yet known and different candidates were more particularly proposed in the study by Balasubramanian et al.[71] The (possibly) MgV center was also recently discovered (ZPL at 557 nm) and is currently under theoretical considerations regarding its spin properties and charge states. It was created in intrinsic diamond with efficiencies of 12% at 1600 °C[47] or 8.7% at 1200 °C.[14]

Apart for the NV and SiV centers, the energy and fluence dependence data are not available. Nevertheless, the yield of a few percent is a common feature to column IV-vacancy centers, despite their different impurity atomic mass of 28, 72.6, 118.7, and 207.2 which may lead to strongly different defect configurations around the implanted atoms.[47] Not only for the NV center but also for defects involving two vacancies (in the split-vacancy impurity model), all these results confirm that vacancy is the limiting process to a high efficient impurity-vacancy centers formation. This is mainly owing to vacancy–interstitial recombination and to the robust formation of V_n complexes. As discussed, the larger the atom, the larger and more numerous vacancy complexes are created, keeping isolated vacancies unavailable.

3.3. Diffusion in Diamond

Diffusion in diamond is extremely low compared with other materials and the determination of the diffusion coefficient of the different species is difficult. This makes it, however, a great advantage for applications with color centers which are, as a consequence, extremely temperature- and photostable. **Figure 5** shows the diffusion coefficient measured experimentally for vacancies, hydrogen, and nitrogen. It can be seen at first sight that the values cover several orders of magnitude and that hydrogen is the most mobile species. For most of the results presented here, the diffusion was measured by fitting experimental diffusion profiles of hydrogen (deuterium)[72,73] or passivation of NV centers applying Ficks law in 1D.[47,74] The diffusion length can then be obtained from

$$d \approx \sqrt{Dt} \tag{2}$$

where the diffusion coefficient D is given by

$$D = D_0 \exp\left(\frac{-E_A}{kT}\right) \tag{3}$$

where the activation energy E_A depends on the charge state. Large variations of the diffusion coefficient are observed as a

Figure 5. Diffusion coefficient of hydrogen compared with other often-occurring impurities (vacancy, boron, and nitrogen) in diamond.

function of the diamond doping type[75] or applying an electrical bias.[72] No H diffusion could be observed in n-type diamond, up to 1000 °C, whereas it is significant in p-type diamond. These results show that it is therefore possible to control H diffusion in view of a possible advanced defect engineering. It is also known that hydrogen binds likely to many species, especially boron[73] or nitrogen,[76] which can thus limit the diffusion. The high value obtained in the study by Stacey et al.[74] in undoped IIa diamond under H plasma exposure was not confirmed by similar measurements done in the study by Lühmann et al.[47] However, a similar large-scale (tens of μm) surface-related depletion was reported in the study by Chakravarthi et al.[77] during thermal annealing but without any H plasma applied.

The diffusion of isolated neutral vacancies is two to four orders of magnitude less than for hydrogen. It was mostly determined by the formation of NV centers from native nitrogen atoms in irradiated diamonds. The D value is $>1\,\mathrm{nm}^2\,\mathrm{s}^{-1}$ at 850–1000 °C[55,78] with E_A about 2.12 eV. It is large enough to ensure the diffusion of one of the induced vacancies toward the implanted nitrogen in the case of N implantation (Section 3.1). The fact that the NV creation efficiency is only of a few percent is a clear signature that there are competing defects which form, such as divacancies or larger vacancy complexes and which are highly temperature stable.[51,79] In diamond of type IIa and IIb (with $[B] = 9 \times 10^{17}\,\mathrm{cm}^{-3}$) irradiated with MeV electrons, it was shown that, in the temperature range 600–850 °C, the loss of isolated neutral vacancies V^0 (GR1) correlates with the appearance of V^0–V^0 (TH5a, M1, M2).[80,81] In type Ib diamond, the annealing of negatively charged vacancies V^- takes more time than for V^0 and it was found that V^- is destroyed first by being converted to V^0.[82] Note that is was found using MD simulations[48] that vacancy diffusion near a diamond surface has a lower diffusion barrier (0.42 eV) than in the bulk (1.7–2.8 eV).[83–85]

The diffusion of carbon interstitials is larger than for vacancies[86,87] and has an activation energy of 1.56–1.74 eV.[88] The interstitial–vacancy recombination process (after a 2 MeV electron irradiation with fluence $1 \times 10^{18}\,\mathrm{cm}^{-2}$) was determined in type IIa diamond at 460 °C: about 20% of the pairs have

recombined after 1 h. The interstitial absorption (R2) anneals completely between 400 and 500 °C for longer times, whereas the vacancy absorption is only partly reduced. The situation is different in type Ib diamond (rich in isolated nitrogen which is a deep donor). The Frenkel pairs dissociate above 350 °C giving rise to isolated negative vacancies V^- (ND1) and carbon interstitials I^0 (R2).[87] Above 500 °C, the R2 absorption anneals out without any change in the ND1 absorption intensity.

Finally, the diffusion of nitrogen is considerably less and was deduced from the dissociation of NVs and the formation of NVN (H3) centers at large temperature ($1.7 \times 10^{-3}\,\mathrm{nm}^2\,\mathrm{s}^{-1}$ at 1600 °C) and large nitrogen content.[47,89] In such a process, it is therefore assisted by the presence of a vacancy and it is larger than the migration of the single nitrogen atom.[90,91]

3.4. Hydrogen in Diamond

The highest purity samples needed for diamond-based quantum applications possess impurity contents of nitrogen and boron typically below the detection limit of standard measurement methods such as electron paramagnetic resonance (EPR) or Fourier-transform infrared spectroscopy. They are generally grown using plasma-assisted chemical vapor deposition (PA-CVD), whereas the HPHT synthesis gives rise to still larger boron contents. Even if diffusion in diamond is low compared with other materials, it was shown in the previous section that hydrogen diffusion is significant, and depends on its charge state, H^+, H^0, or H^-. The continuous exposition of the on-growing crystal (which is generally kept at temperatures of 750–900 °C) to hydrogen plasma in PA-CVD inevitably induces a hydrogen contamination. It is, however, difficult to estimate the hydrogen content and homogeneity because it is difficult to detect by conventional methods. The sensitivity of secondary ion mass spectroscopy (SIMS) for hydrogen is limited to about $10^{18}\,\mathrm{cm}^{-3}$ (6 ppm)[92] and it is similar and about 1 ppm for nuclear reaction analysis (NRA). Nevertheless, it can be considered that hydrogen is the most common impurity in CVD diamond and it needs to be taken into account for the creation and application of color centers, or for efficient doping, as it will be shown in the following. Hydrogen binds easily not only to boron,[73] to nitrogen[76,93] but also to NV and forms NVH (which has a 1 eV lower formation energy than NV[94]). There is also experimental evidence of NV passivation by hydrogen.[47,74,77,95] In CVD-grown diamond, the NVH concentration is always typically at least one order of magnitude larger than the NV concentration, whatever the nitrogen impurity concentration.[96,97]

4. Charge-Assisted Defect Engineering

The main competitors for the formation of impurity-vacancy centers are divacancies[47] or larger vacancy clusters, and in the case of NV centers, NVH complexes can also form.[94,96] To prevent the formation of V_2 and V_n, it was proposed to take advantage of Coulomb repulsion forces and to charge vacancies negatively using n-type doping[14] or positively using p-type doping.[50,98] Charging defects before and during the thermal annealing likely modifies the diffusion properties and defect formation. Here, we describe the results obtained by charging vacancies (and other

defects) and discuss the properties of the NV centers at the single level to infer about the formation mechanisms. This technique is at its beginning but opens the way to an advanced engineering of single defects in the solid-state and not only diamond.

4.1. Which Donor to Use?

Although p-type doping using boron is well established, the obtention of n-type conductivity by CVD was long an issue[92,99] and it was never really achieved by ion implantation.[100] Phosphorous is to date the donor of choice for n-type within electronic devices,[101] but it has a relatively large ionization energy ($E_d = 0.57$ eV) and the search for an alternative and shallower donor is still open. With an even deeper state ($E_d = 1.7$ eV),[102] Nitrogen is still considered as a donor, especially because it is the main contributor to the negative charge state of NV⁻ centers in most of experimental situations.[103,104] Lithium implantation was shown to give rise to n-type conductivity,[105] but it is owing to interstitial lithium (the n-type behavior disappears after annealing) which is not suitable for this study because the color centers creation requires a thermal treatment. Oxygen and sulfur are expected to be double donors with acceptable size to fit in substitutional sites. In the case of Sulfur, it was predicted that only substitutional S_s and V–S–V defects should survive the postimplantation annealing.[106] Saada et al.[107] calculated that the energy levels of S^0 and of S^+ should lie 0.15 and 0.50 eV below the conduction band minimum. However, the lowest formation energy of S^{2+} likely implies that only a low number of active S centers may be found.[107] In addition, the (VSV)⁻ defect is expected to be an acceptor, thus compensating the S donor,[106] whereas the S–H defect is expected to be a shallow donor.[108] N-type conductivity caused by a sulfur-related mechanism (with an activation energy of 0.5–0.75 eV above 600 K) was reported in the study by Nakazawa et al.[109] in S-doped CVD diamond. Using oxygen implantation and low-temperature annealing at 500 °C, n-type was reported with an activation energy of 0.32 eV.[110]

4.2. Charging Vacancies

The idea behind the first attempt of lattice charging[50] is to use a thin sacrificial layer of highly boron-doped material and to produce NV centers a few nm below this layer by nitrogen implantation. The depletion layer formed at the p^+-type to intrinsic junction induces a band bending producing a positive charging of the implantation-induced vacancies (expected to be in the 2+ charge state). The boron-doped layer was produced by CVD growth, and had a thickness of 6 nm and a boron concentration of 1×10^{20} cm⁻³. The nitrogen energy ranged between 2.5 and 9.8 keV. The sample was annealed at 950 °C for 2 h. After this, the boron-doped layer was removed by a 7 nm deep etching. A reference sample without doped layer was produced for comparison. In this work, there was no direct evidence of the charging of vacancies into V^+ or V^{2+} but indirect effects were observed on the NV creation efficiency (Section 4.3) and on the coherence properties of the NV centers (Section 4.4). Both were improved, which can be explained by a reduction of the divacancy formation. Kinetic Monte Carlo simulations were showing that

otherwise (in intrinsic diamond) 30–40% of the produced vacancies were aggregating into V_2 or larger clusters after annealing.

The second approach consists in the creation of NV, SnV, and MgV centers into a material previously doped with donors.[14] This first proof-of-principle experiment was done using phosphorous. Different sectors of a same diamond sample were prepared by implantation of dopants and thermal annealing. Boron was also implanted as comparison, and nonintentionally doped diamond was considered as intrinsic. Carbon was then implanted in the different sectors to produce vacancies for spectroscopic investigation of their charge state using a confocal fluorescence microscope. The PL emission of V^0 (GR1) has a characteristic ZPL at 741 nm, whereas V^+ has no known optical signatures and V^- (ND1) is present in absorption at 394 nm.[53] The results are shown in **Figure 6**a, which is a confocal scan of the unannealed carbon implantations where the fluorescence is spectrally filtered to observe V^0. There is no V^0 fluorescence in the phosphorous-doped area, whereas V^0 is visible in the intrinsic region and strongest in the B-doped one (Figure 6b). With the help of Figure 6c, it can be deduced that the vacancies are negatively charged in the phosphorous area, have a mixed charge state in the intrinsic region, and are mainly neutral in the boron-doped one. Note that even if the vacancy charge state can be predicted by the Fermi-level position, the laser excitation used for the measurement cannot be neglected. Interestingly, it can also be noted that the amorphization threshold of diamond is increased in the donor-doped area (as seen for the 2×10^{12} cm⁻² carbon fluence), which is likely due to the mutual repulsion of the negatively charged vacancies, preventing vacancy aggregation. It was also observed in this sample the presence of 3H centers (split interstitial related[47]) only in the donor-doped region. This is in good agreement with the enhanced dissociation of Frenkel defects reported for n-type diamond (Section 3.3). Note that hydrogen diffusion is expected to be inhibited in the P-doped areas.

4.3. Highly Enhanced NV Center Formation

The consequence of the pining of the Fermi level and vacancy charging can be directly observed on the NV creation efficiency. The typical NV yield versus ion energy dependence for intrinsic diamond and standard annealing conditions (800–900 °C for a few hours) is shown in **Figure 7**d (gray dots and line). In the case of the p^+–i junction and its control reference experiment,[50] the nitrogen implantation energy was below 10 keV. This gives rise to NV depths of 5–20 nm and creation yields in the percent range or less. The results are shown in Figure 7d (green circles). The NV yield is improved by about a factor of two (slightly depending on ion energy and fluence) with the help of the vacancy charging.

In the codoping approach of Lühmann et al.,[14] a slightly larger depth (40 nm) was chosen to avoid surface effects. A sketch of the method is shown in Figure 7a. Two samples were prepared, with different annealing conditions for the dopants: 1600 °C for 4 h with P and B for the first one and 1200 °C for 4 h with P, S, and O for the second one. In view of the hydrogen diffusion described in Section 3.3, the electrical activation or passivation of the dopants may be strongly influenced by the temperature chosen. Different atoms were then implanted in the three regions (and further annealed): nitrogen for NVs but also
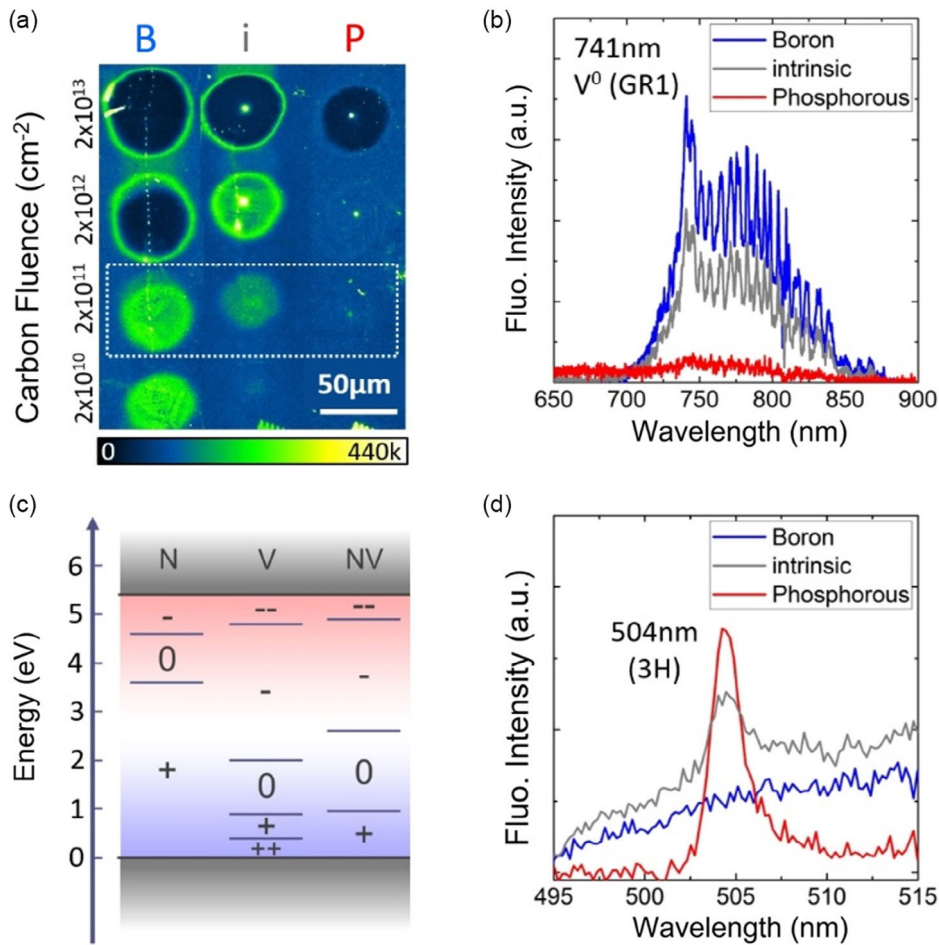
Figure 6. Charging single vacancies prior to annealing. a) Confocal fluorescence scan of carbon implantations (spots of 50 μm diameter) into three different doped regions: p-type, intrinsic and n-type with [B] and [P] about 3×10^{18} cm^{-3}. Laser excitation at 532 nm and detection window 700–800 nm. b) Fluorescence spectra recorded in the three doped areas for the 2×10^{11} cm^{-2} carbon fluence (acquisition by scanning a 10×10 μm^2 area at the center of each spot). The characteristic emission from the V^0 at 741 nm is recognized. a,b) Reproduced under the terms of the Creative Commons Attribution 4.0 license.[14] Copyright 2019, The Authors. Published by Springer Nature. c) Charge transition levels of nitrogen, vacancies, and NV center calculated ab initio by Deak et al.[94] d) Fluorescence spectra (with 488 nm excitation) after 800 °C annealing revealing 3H centers at 504 nm.

Sn and Mg for SnV and MgV centers, and carbon as reference. For the first sample, the NV yield presents a threefold improvement from 7% (intrinsic) to 22.7% (P-doped) whereas it is reduced for B-doping (Figure 7b). This can be well understood in view of the results shown in Figure 6a: the vacancies are neutral in the B-doped area (forming complexes) and negatively charged in the P-doped one (staying isolated and available to form NVs). The yield improvement vanishes when the nitrogen fluence increases, that is when the number of vacancies to be charged surpasses the number of active donors available. For the dopants annealed at 1200 °C, the yield improvement is tenfold, as seen in the fluorescence scans in Figure 7c,d, where it is of 60% for P-doping, 70% for O-doping, and up to 75% for S-doping. Note that a few NVs are created from native nitrogen impurities but their number is easy to estimate and is negligible with respect to the implanted N to NV process. In addition, it cannot be fully ruled out that a part of the NVs is benefiting from unhealed vacancies induced by the donor implantation.

These very high yield values are bringing the NV scalability closer to a real deterministic creation. They also indicate that oxygen and sulfur behave at first sight as phosphorous. The next question is whether the two methods also provide NV centers with high optical and spin properties, that is, with a "clean" environment and with good charge state stability. Especially, the sacrificial B-doped layer must be properly and fully removed[50] and the presence of the donors[14] must not contribute to a loss of the NV spin coherence or to a higher charge tunneling rate.

As discussed in more details in Section 4.4, the creation yield of MgV and SnV centers is also enhanced by a factor of 3–6 using phosphorous doping. Recently, it was reported that the formation of implanted SiV^0 can be very high in CVD boron-doped diamond (with [B] = 1–3 ppm).[98] Despite a laser-induced blinking of single centers, the acceptors not only strengthen the SiV^0 neutral state (as already observed in the study by Groot-Berning et al.[111]) but also charge the implanted vacancies positively in the low Si fluence regime.
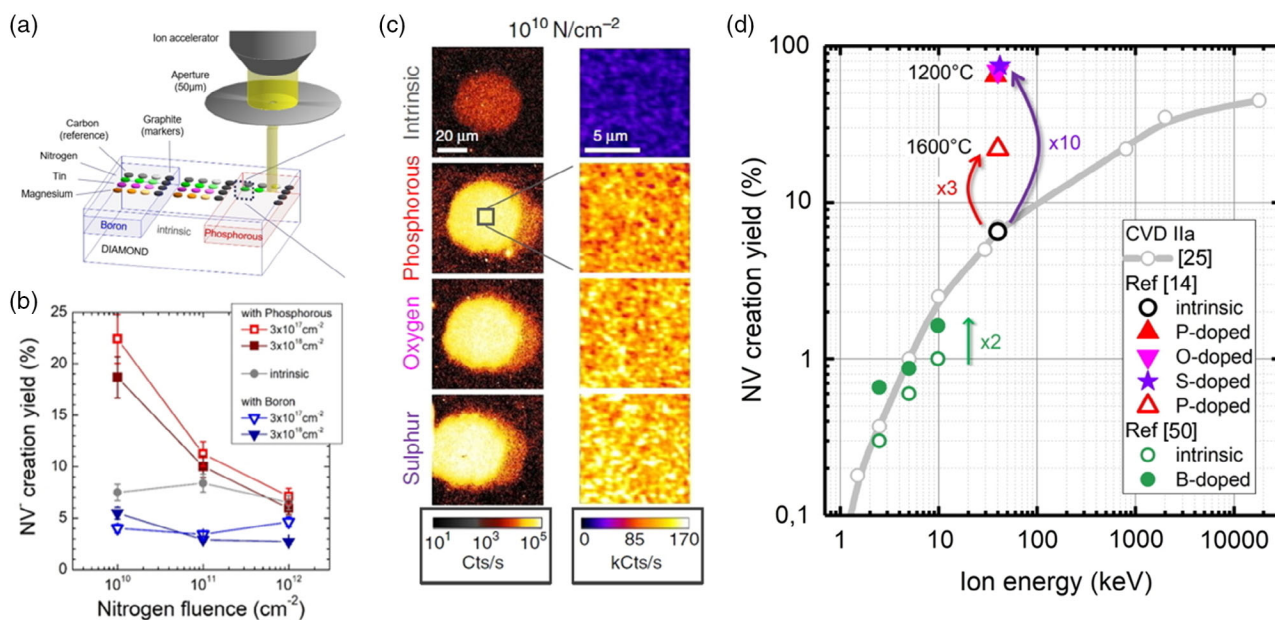
Figure 7. Charge-assisted NV creation enhancement. a) Scheme of the diamond sample used for the proof-of-principle experiment. Areas are prepared with intrinsic, p-type, and n-type doping (here boron and phosphorous). The sample is annealed to activate the dopants and in a second step the color centers are implanted in each zone and annealed. b) NV creation yield as a function of the nitrogen fluence for different diamond doping (dopants annealed at 1600 °C). c) Confocal scans of implanted NV centers for different donors, compared with intrinsic diamond (dopants annealed at 1200 °C). a–c) Reproduced under the terms of the Creative Commons Attribution 4.0 license.[14] Copyright 2019, The Authors. Published by Springer Nature. d) Creation efficiency of NV centers as a function of the ion kinetic energy in standard annealing conditions. The gray curve represents the typical and widely reproducible values in IIa diamond. The green dots are from the study by Fávaro de Oliveira et al.,[50] where the sacrificial B-doped top layer is used and compared with intrinsic diamond. The other symbols at the energy of 40 keV are from the study by Lühmann et al. [14] using donor doping.

4.4. Charge State and Coherence Time

It is admitted that an NV center requires a close-by donor to be negatively charged.[103,104] Most NV applications rely on the negatively charged state and any ionization, instability, or blinking is detrimental for their good operation. Owing to intrinsic photo-ionization processes, single NV centers undergo, however, continuous ionization and recharging cycles under laser excitation.[112] Several works show that the use of donor doping brings a larger NV$^-$ content in ensembles or more time spent in the NV$^-$ state for single NVs.[20,111,113] The random local effect of the donor position relative to the NV center is evidenced in **Figure 8**a, which shows the radically different charge state interconversion of two single NV centers separated by less than 2 µm in the same phosphorous-doped layer (5×10^{16} cm^{-3}).[113] In Manson et al.,[104] new insights in the NV$^-$–N$^+$ pair and electron tunneling dynamics are given, especially highlighting the effect of the NV–N distance and the laser wavelength excitation. It is, moreover, shown how a too large donor concentration (or too short NV–N separation) leads not only to a PL quenching but also to a reduction of the ODMR contrast (Figure 8f). Mittiga et al.[114] reported that the NV–N pair can be stable over months in a IIa diamond, i.e., the same nitrogen atom is ionized and a 3D localization with respect to the NV center is shown in Figure 8e.

In the work of Herbschleb et al.,[20] the highest NV coherence is reported in slightly phosphorous-doped CVD diamond (3×10^{15} cm^{-3} < [P] < 1×10^{17} cm^{-3}), from native isolated NVs. A rough correlation between NV$^-$ stability and spin coherence is shown: the largest T_2 are obtained for 100% NV population (Figure 8d). In the work of Favaro et al.,[50] it is mandatory to etch away the sacrificial highly boron-doped layer to recover a Fermi-level position suitable for having negatively charged NV centers. In the work of Lühmann et al.,[14] the NV charge state was measured for low-density NV ensemble as a function of the donor species used (annealed at 1200 °C). The results are shown in Figure 8b, together with intrinsic and B-doped diamond for comparison. Sulfur doping gives rise to a more negative state than oxygen and phosphorous doping. It is believed that the donors charge all possible deeper states (acceptors for NVs) which could lead to NV$^-$ ionization. Figure 8c shows the acceptor effect of single vacancies on the NV charge state. Here, the difference between the emission spectra of the same NV ensemble is shown after an 800 °C annealing (where [V] ≤ [NV]) compared with the previous situation for a 600 °C annealing (where [V] ≫ [NV]). The annihilation of vacancies at 800 °C enables a mainly NV$^-$ state, whereas a dominant NV^0 state is observed at 600 °C.[14]

The consequences of the lattice charging of Fávaro de Oliveira et al.[50] are clearly observed on the spin properties of the NV centers, which are excellent sensors of their own local environment. By comparing NV centers at the same depth in the reference sample and in the p$^+$–i junction sample (after etching of the top Boron-doped layer), a tenfold improvement of T_2 times is found for shallow NVs of depth < 5 nm. T_1 times are as well
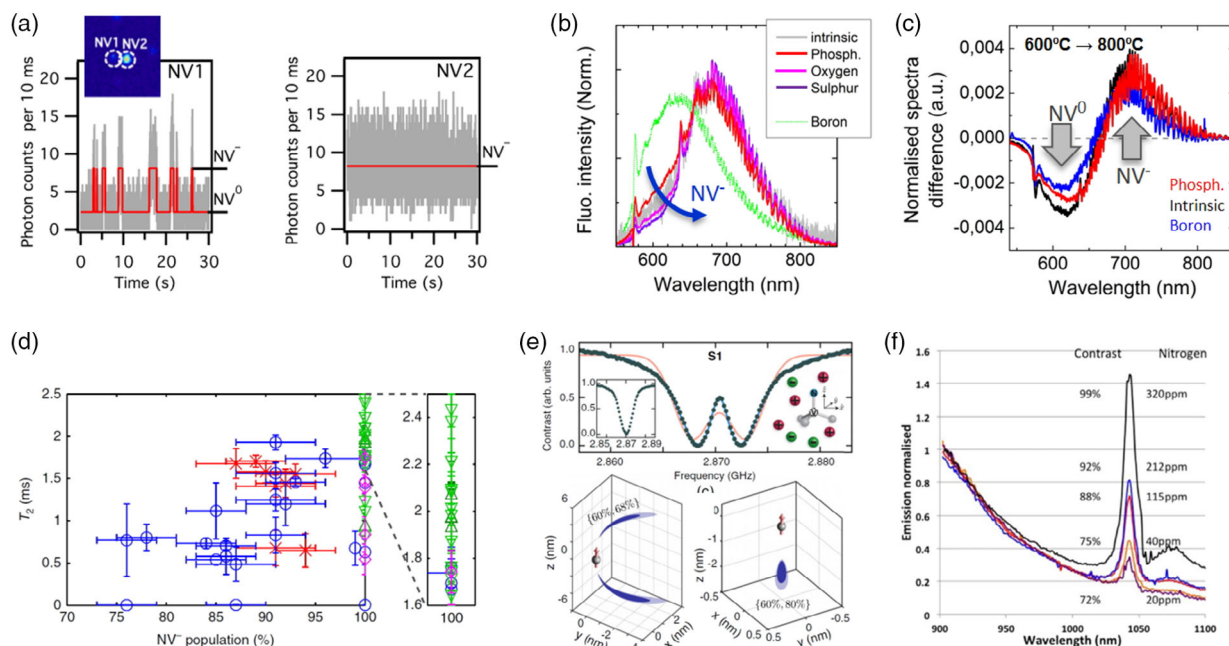
Figure 8. NV charge state. a) Fluorescence time traces of two individual NV centers (separated by less than 2 μm) in a phosphorous-doped diamond ($[P] = 5 \times 10^{16}$ cm^{-3}). Reproduced with permission.[113] Copyright 2016, American Physical Society. b) Average charge state of an ensemble of NV centers created using the Coulomb-driven method, for different donors, for intrinsic diamond and for boron-doped. Reproduced under the terms of the Creative Commons Attribution 4.0 license.[14] Copyright 2019, The Authors. Published by Springer Nature. c) Difference of the PL spectra of the same NV ensembles (in P-doped [red], B-doped [blue], and intrinsic [black] diamond) annealed at two different temperatures for 4 h each: PL (800 °C)–PL (600 °C). The shift from NV^0 to NV$^-$ between 600 and 800 °C is owing to the annealing of vacancies which are acceptors for the NVs. d) Coherence time T_2 of several individual NV centers as a function of their NV$^-$ population. Reproduced under the terms of the Creative Commons Attribution 4.0 license.[20] Copyright 2019, The Authors. Published by Springer Nature. e) Imaging of the close-by ionized nitrogen donor (using the NV center itself) reveals that it is the same nitrogen atom which "gives" its electron for several months. Reproduced with permission.[114] Copyright 2018, American Physical Society. f) Emission intensity of the IR transition of an ensemble of NV centers as a function of the nitrogen content (i.e., average NV to N distance), revealing a loss of the ESR contrast when [N] increases. Reproduced under the terms of the Creative Commons Attribution 3.0 license.[104] Copyright 2018, The Authors. Published by IOP Publishing.

improved. These findings, together with their depth dependencies and MD simulations, are well explained by the suppression of the formation of divacancies, which are paramagnetic centers.[51] Furthermore, noise spectroscopy[115] was conducted to analyze the magnetic noise experienced by the NVs in each sample. The noise spectra of 3 nm deep NVs are shown in **Figure 9**a. With a fine analysis of the different noise contributions (the density of surface spins was estimated to be about 10^{13} cm^{-2}), it was concluded again that the signature of V_2 electron spins is suppressed when the p$^+$–i junction method is used. This is an indirect proof that the vacancies were properly positively charged.

In the work of Lühmann et al.,[14] the NV centers were implanted deeper (40 nm) to minimize the effect of surface charges and spins and to account only for the doping effect on the NV creation yield and properties. T_2^* and T_2 times were measured at 300 K on several NV centers in the areas predoped with different species and in the nondoped (intrinsic) area. These results are shown in Figure 9b and compared with the coherence properties of CVD-grown NVs in intrinsic[116] and in lightly phosphorous-doped diamond.[20] As expected, the implanted NVs in intrinsic diamond have shorter coherence times than CVD-grown NVs (for similar nitrogen concentration) owing to remaining implantation defects. The donor species conduct to

significantly different T_2 times: 4.8–14 μs for phosphorous, 19–55 μs for oxygen, and 34–110 μs for sulfur. Compared with a nitrogen-concentration-equivalent T_2 of 15–25 μs, it corresponds to a fivefold improvement for sulfur, whereas phosphorous leads to a twofold decrease. Interestingly, the moderate phosphorous doping by CVD growth used by Herbschleb et al. gives the longest T_2 and T_2^* reported for isolated native NV centers.[20] It would be of interest to vary and especially to reduce the sulfur doping level (and nitrogen implantation fluence) to further enhance the coherence times of implanted NV centers. More theoretical and experimental works are required regarding the electronic and spin configuration of donor atoms and of their complexes such as a stable S–H pair which may be a shallow donor[108] or (V–S–V)$^-$ which likely compensates substitutional S.[106] Used as sensors and/or electrical traps, the NV centers may give new insights in n-type doping of diamond, more particularly concerning the charge state and spin of S and O impurities.

Further works are necessary also regarding the optimal conditions for the donor doping itself, to obtain the highest electrical activation possible.[100,117,118] A compromise is likely to be found, especially between the correct placement in substitutional site and the passivation by hydrogen or vacancy capture. For boron
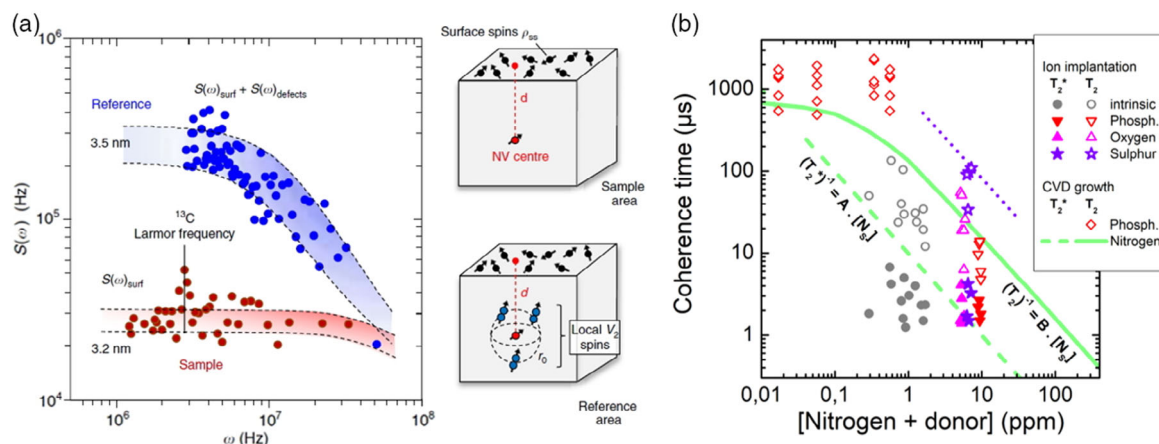
Figure 9. NV environment. a) Noise spectra sensed by two different NV centers implanted without (reference, blue dots) and with the p^+–i method (sample, red dots) from the study by Fávaro de Oliveira et al.[50] at the same depth of 3 nm. The two situations are illustrated on the corresponding schemes and the difference in noise intensity is attributed to the presence or the suppression of V_2 electron spins. Reproduced under the terms of the Creative Commons Attribution 4.0 license.[50] Copyright 2017, The Authors. Published by Springer Nature. b) Coherence times T_2 and T_2^* of several NV centers as a function of the sum of implanted nitrogen and donor concentrations, following the method from the study by Lühmann et al.[14] The green reference lines are for CVD-grown NV centers from the study by Barry et al.[116] The extra points (red rhombus) are extracted from the study by Herbschleb et al.[20] for CVD-grown NVs and P doping. Reproduced under the terms of the Creative Commons Attribution 4.0 license.[14] Copyright 2019, The Authors. Published by Springer Nature.

doping by implantation, an electrical activation of 10–15% only (ratio of hole concentration and boron concentration) was reported for 1600 °C annealing.[119,120] For phosphorous implantation and 1600 °C annealing, 70% of the atoms were found in substitutional sites.[121] This is comparable with what was found for N implantation (50%)[122] and S implantation after a 800 °C annealing (50%).[118]

4.5. What Are the Best Conditions?

In view of the competing defect formation, the variety of involved species, the doping type, the local Fermi level position, the local strain, the hydrogen content, and so on, it seems that the efficient engineering of high-quality color centers requires a specific recipe for each center and targeted application, to be found within an unlimited number of combinations. This is evidenced in **Figure 10**a, where the formation of three kinds of color centers (NV, SnV, and MgV) is compared within the same sample and the same conditions.[14] Although the thermal stability of NVs was demonstrated up to about 1300 °C,[47,53] it can be seen that the NV density in the intrinsic and B-doped areas is reduced by more than one order of magnitude between 800 and 1000 °C. In contrast, the NV density slightly increases in the P-doped zone of the same diamond. In addition, the density of SnV and MgV is constant or increases. If the temperature is further increased to 1200 °C, the NV loss continues whereas the SnV and MgV formation keeps increasing. The most probable reason for this is the passivation by hydrogen of NV centers but not of SnV and MgV. The radically different behavior in n-type diamond is in good agreement with the doping-dependent H diffusion reported by Saguy.[75] Regarding the capture of hydrogen by NV centers, it was evidenced experimentally that nitrogen is an even more efficient trapping center. This can be seen in Figure 10b and found in more details in the studies by Lesik et al.[95] and Lühmann

et al.[47] The NV survival to H passivation increases when the [N]/[NV] ratio increases. Owing to the strong NV yield versus ion energy dependence, more N are required to produce one NV when the energy is reduced (for shallower NVs). The survival of the shallowest NVs to hydrogen plasma exposure can be explained by a more efficient H capture by the excess nitrogen. This gives an interesting possibility to prepare H traps to protect the color centers from H diffusion from the outside. In Figure 10c, the NV passivation is summarized for several conditions of NV depth, density, and H plasma conditions.[47] A similar experiment was conducted by directly implanting hydrogen into preexisting NV ensembles followed by a thermal treatment to enable hydrogen diffusion. Similarly, the NV survival increases with the initial nitrogen fluence, as shown in Figure 10e.

From the point of view of the spin coherence properties, it was shown that the optimal temperature regarding the elimination of most of the paramagnetic defects (measured in EPR and correlated to T_2 increase) was at about 1050 °C.[51,123] At higher temperatures, the vacancy chains transform to vacancy rings which are even more detrimental for the NV coherence time. This was, however, measured for deep NVs implanted at 2 MeV. In the case of shallow NV centers, the surface proximity and possibly different diffusion constants may require the use of other conditions.

Recently, a large-scale study of the NV centers kinetics was conducted on thousands of individual NVs in IIa diamond,[77] confirming the NV passivation by H and evidencing its coexistence with NV formation and orientation change depending on the temperature. In this work, the NV passivation by H has two causes: a surface-driven diffusion (for several tens of μm) and the release of H from NVH_x complexes.[124,125]

Controlling further the different competing processes of defect formation will be beneficial not only for the color centers applications but also for the diamond doping as well. In this view,
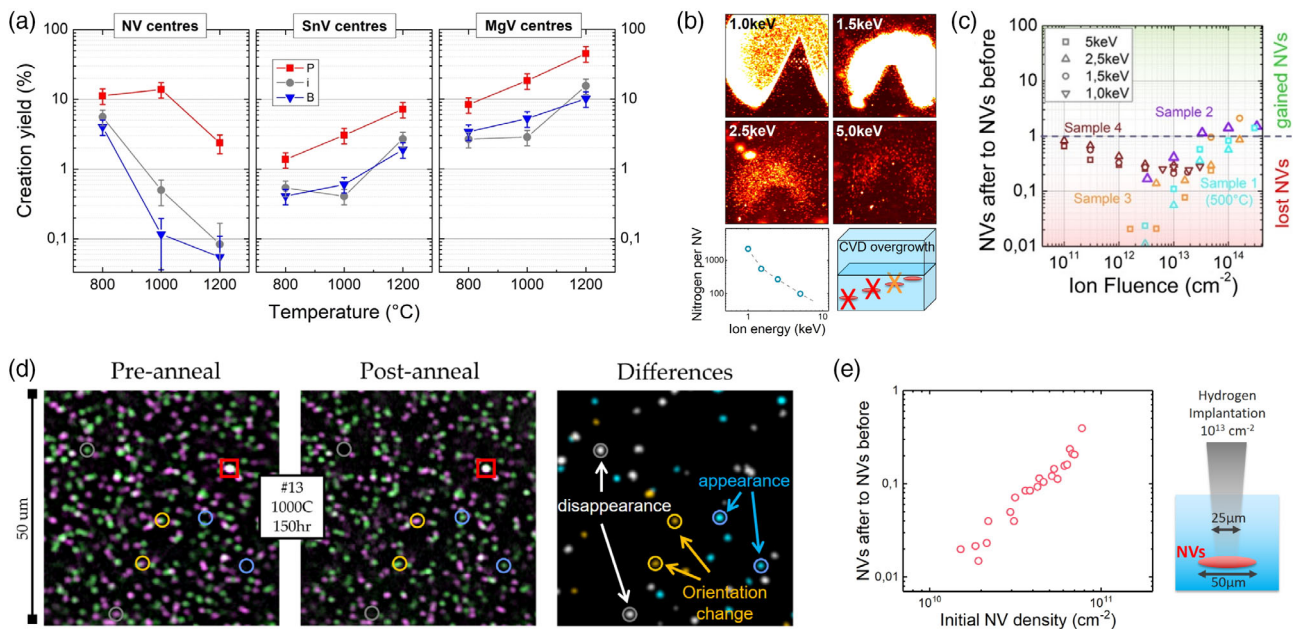
Figure 10. Temperature treatment. a) Effective creation yield of NV, SnV, and MgV centers as a function of consecutive thermal treatments (4 h each) and doping type within the same diamond. Reproduced under the terms of the Creative Commons Attribution 4.0 license.[14] Copyright 2019, The Authors. Published by Springer Nature. b) Confocal fluorescence scans of implanted NVs (at 1.0, 1.5, 2.5, and 5.0 keV) after CVD overgrowth. NV centers are lost by hydrogen passivation and NVH formation owing to H diffusion during the overgrowth process. Shallower NVs are preserved because they needed a larger number of nitrogen to be implanted and because N atoms trap H efficiently.[47,95] c) Loss and gain of NV centers for different CVD overgrowth and hydrogenation experiments. b,c) Reproduced with permission.[47] Copyright 2018, IOP Publishing. d) Spatial tracking of NV centers revealing appearances, disappearances, and orientation changes during thermal annealing. Reproduced with permission.[77] Copyright 2020, American Physical Society. e) Targeted implantation of hydrogen into a preexisting NV centers ensemble. The energy was set to 5 keV to reach the 50 nm deep NV centers and the fluence was 10^{13} cm^{-2}. The survival of NVs (after H implantation and thermal annealing at 800 °C in vacuum for 2 h) is plotted as a function of the initial NV density.

the use of electrical bias, light illumination, rapid thermal annealing, or traps for diffusing species may improve and refine further the promising results of charge-assisted defect engineering.

5. Conclusion

With the emergence of implantation techniques providing the deterministic implantation of countable ions of any kind and with a high spatial resolution, new perspectives are opened for low-dimension devices where the number and positioning of dopants becomes critical. With such techniques, the hardware of a solid-state quantum computer can be scaled up, provided that the implanted ions can as well be transformed into usable objects, i.e., qubits, with optimal properties. The recently developed methods of charge-assisted defect engineering bring defect centers in the solid-state closer to a full deterministic creation. By modifying the defect formation and diffusion, they give a new degree of freedom for the enhanced creation of specific centers and for the control of their environment.

Applied to NV centers in diamond, a tenfold better creation yield up to 75% was demonstrated. Moreover, a better charge state stability and longer spin coherence time were achieved, both critical for quantum sensing or information processing applications. The same effect of enhanced creation was observed for other color centers such as the SnV or MgV, which

demonstrates the versatility and interest of the method for other materials or defect centers. Furthermore, the method helped highlight the critical role of hydrogen in diamond and gives hints how to reduce its effect by playing with a large number of parameters (doping, annealing temperature and time, applied bias, light illumination, addition of specific trapping centers, etc.).

Together with other recent breakthroughs achieved in the individual addressing/readout of single centers and in the scalability using the coupling to nuclear spins, the feasibility of a diamond-based quantum computer is at a watershed. Despite the large advance taken by the superconducting qubits and ion traps technologies, the NV center in diamond system is still the only candidate for room-temperature operation, and it offers scalability, robustness and cost-effectiveness inherent to single defects in a solid-state system.

Conflict of Interest

The authors declare no conflict of interest.

Keywords

creation yield, deterministic creation, diamond, ion implantation, nitrogen-vacancy center, qubit

[1] A. Gruber, A. Dräbenstedt, C. Tietz, L. Fleury, J. Wrachtrup, C. von Borczyskowski, *Science* **1997**, *276*, 2012.

[2] F. Jelezko, T. Gaebel, I. Popa, A. Gruber, J. Wrachtrup, *Phys. Rev. Lett.* **2004**, *92*, 076401.

[3] T. D. Ladd, F. Jelezko, R. Laflamme, Y. Nakamura, C. Monroe, J. L. O'Brien, *Nature* **2010**, *464*, 45.

[4] G. Balasubramanian, P. Neumann, D. Twitchen, M. Markham, R. Kolesov, N. Mizuochi, J. Isoya, J. Achard, J. Beck, J. Tissler, V. Jacques, P. R. Hemmer, F. Jelezko, J. Wrachtrup, *Nat. Mater.* **2009**, *8*, 383.

[5] G. D. Fuchs, V. V. Dobrovitski, D. M. Toyli, F. J. Heremans, D. D. Awschalom, *Science* **2009**, *326*, 1520.

[6] F. Dolde, I. Jakobi, B. Naydenov, N. Zhao, S. Pezzagna, C. Trautmann, J. Meijer, P. Neumann, F. Jelezko, J. Wrachtrup, *Nat. Phys.* **2013**, *9*, 139.

[7] L. Rondin, J.-P. Tetienne, T. Hingant, J.-F. Roch, P. Maletinsky, V. Jacques, *Rep. Prog. Phys.* **2014**, *77*, 056503.

[8] F. Dolde, H. Fedder, M. W. Doherty, T. Nöbauer, F. Rempp, G. Balasubramanian, T. Wolf, F. Reinhard, L. C. L. Hollenberg, F. Jelezko, J. Wrachtrup, *Nat. Phys.* **2011**, *7*, 459.

[9] M. Lesik, T. Plisson, L. Toraille, J. Renaud, F. Occelli, M. Schmidt, O. Salord, A. Delobbe, T. Debuisschert, L. Rondin, P. Loubeyre, J.-F. Roch, *Science* **2019**, *366*, 1359.

[10] G. Kucsko, P. C. Maurer, N. Y. Yao, M. Kubo, H. J. Noh, P. K. Lo, H. Park, M. D. Lukin, *Nature* **2013**, *500*, 54.

[11] T. Staudacher, F. Shi, S. Pezzagna, J. Meijer, J. Du, C. A. Meriles, F. Reinhard, J. Wrachtrup, *Science* **2013**, *339*, 561.

[12] F. Arute, K. Arya, R. Babbush, D. Bacon, J. C. Bardin, R. Barends, R. Biswas, S. Boixo, F. G. S. L. Brandao, D. A. Buell, B. Burkett, Y. Chen, Z. Chen, B. Chiaro, R. Collins, W. Courtney, A. Dunsworth, E. Farhi, B. Foxen, A. Fowler, C. Gidney, M. Giustina, R. Graff, K. Guerin, S. Habegger, M. P. Harrigan, M. J. Hartmann, A. Ho, M. Hoffmann, T. Huang, et al., *Nature* **2019**, *574*, 505.

[13] K. Groot-Berning, T. Kornher, G. Jacob, F. Stopp, S. T. Dawkins, R. Kolesov, J. Wrachtrup, K. Singer, F. Schmidt-Kaler, *Phys. Rev. Lett.* **2019**, *123*, 106802.

[14] T. Lühmann, R. John, R. Wunderlich, J. Meijer, S. Pezzagna, *Nat. Commun.* **2019**, *10*, 4956.

[15] Y. C. Chen, B. Griffiths, L. Weng, S. S. Nicley, S. N. Ishmael, S. Johnson, C. J. Stephen, B. L. Green, G. W. Morley, M. E. Newton, M. J. Booth, P. S. Salter, J. M. Smith, *Optica* **2019**, *6*, 662.

[16] P. Siyushev, M. Nesladek, E. Bourgeois, M. Gulka, J. Hruby, T. Yamamoto, M. Trupke, T. Teraji, J. Isoya, F. Jelezko, *Science* **2019**, *363*, 6428.

[17] R. Staacke, R. John, M. Kneiß, M. Grundmann, J. Meijer, *NPJ Quant. Info.* **2019**, *5*, 98.

[18] R. Staacke, R. John, M. Kneiß, C. Osterkamp, S. Diziain, F. Jelezko, M. Grundmann, J. Meijer, *J. Appl. Phys.* **2020**, *128*, 194301.

[19] X. Rong, J. Geng, F. Shi, Y. Liu, K. Xu, W. Ma, F. Kong, Z. Jiang, Y. Wu, J. Du, *Nat. Commun.* **2015**, *6*, 8748.

[20] E. D. Herbschleb, H. Kato, Y. Maruyama, T. Danjo, T. Makino, S. Yamasaki, I. Ohki, K. Hayashi, H. Morishita, M. Fujiwara, N. Mizuochi, *Nat. Commun.* **2019**, *10*, 3766.

[21] C. E. Bradley, J. Randall, M. H. Abobeih, R. C. Berrevoets, M. J. Degen, M. A. Bakker, M. Markham, D. J. Twitchen, T. H. Taminiau, *Phys. Rev. X* **2019**, *9*, 031045.

[22] M. H. Abobeih, J. Randall, C. E. Bradley, H. P. Bertling, M. A. Bakker, M. J. Degen, M. Markham, D. J. Twitchen, T. H. Taminiau, *Nature* **2019**, *576*, 411.

[23] M. Kjaergaard, M. E. Schwartz, J. Braumüller, P. Krantz, J. I.-J. Wang, S. Gustavsson, W. D. Oliver, *Annu. Rev. Condens. Matter Phys.* **2020**, *11*, 369.

[24] S. Pezzagna, J. Meijer, *Appl. Phys. Rev.* **2021**.

[25] S. Pezzagna, B. Naydenov, F. Jelezko, J. Wrachtrup, J. Meijer, *New J. Phys.* **2010**, *12*, 065017.

[26] T. Kornher, K. Xia, R. Kolesov, N. Kukharchyk, R. Reuter, P. Siyushev, R. Stöhr, M. Schreck, H.-W. Becker, B. Villa, A. D. Wieck, J. Wrachtrup, *Appl. Phys. Lett.* **2016**, *108*, 053108.

[27] S. Pezzagna, D. Rogalla, D. Wildanger, J. Meijer, A. Zaitsev, *New J. Phys.* **2011**, *13*, 035024.

[28] N. Raatz, C. Scheuner, S. Pezzagna, J. Meijer, *Phys. Status Solidi A* **2019**, *216*, 1900528.

[29] E. Rittweger, K. Y. Han, S. E. Irvine, C. Eggeling, S. W. Hell, *Nat. Photonics* **2009**, *3*, 144.

[30] S. Pezzagna, D. Wildanger, P. Mazarov, A. D. Wieck, Y. Sarov, I. Rangelow, B. Naydenov, F. Jelezko, S. W. Hell, J. Meijer, *Small* **2010**, *6*, 2117.

[31] J. Riedrich-Moller, S. Pezzagna, J. Meijer, C. Pauly, F. Mucklich, M. Markham, A. M. Edmonds, C. Becher, *Appl. Phys. Lett.* **2015**, *106*, 221103.

[32] P. Spinicelli, A. Dréau, L. Rondin, F. Silva, J. Achard, S. Xavier, S. Bansropun, T. Debuisschert, S. Pezzagna, J. Meijer, V. Jacques, J.-F. Roch, *New J. Phys.* **2011**, *13*, 025014.

[33] D. M. Toyli, C. D. Weiss, G. D. Fuchs, T. Schenkel, D. Awschalom, *Nano Lett.* **2011**, *10*, 3168.

[34] S. Pezzagna, D. Rogalla, H.-W. Becker, I. Jakobi, F. Dolde, B. Naydenov, J. Wrachtrup, F. Jelezko, C. Trautmann, J. Meijer, *Phys. Status Solidi A* **2011**, *208*, 2017.

[35] M. Lesik, P. Spinicelli, S. Pezzagna, P. Happel, V. Jacques, O. Salord, B. Rasser, A. Delobbe, P. Sudraud, A. Tallaire, J. Meijer, J.-F. Roch, *Phys. Status Solidi A* **2013**, *210*, 2055.

[36] S. Becker, N. Raatz, S. Jankuhn, R. John, J. Meijer, *Sci. Rep.* **2018**, *8*, 32.

[37] M. Haruyama, S. Onoda, T. Higushi, W. Kada, A. Chiba, Y. Hirano, T. Teraji, R. Igarashi, S. Kawai, H. Kawarada, Y. Ishii, R. Fukuda, T. Tanii, J. Isoya, T. Ohshima, O. Hanaizumi, *Nat. Commun.* **2019**, *10*, 2664.

[38] T. Matsukawa, T. Fukai, S. Suzuki, K. Hara, M. Koh, I. Ohdomari, *Appl. Surf. Sci.* **1997**, *117*, 677.

[39] T. Shinada, S. Okamoto, T. Kobayashi, I. Ohdomari, *Nature* **2005**, *437*, 1128.

[40] D. N. Jamieson, C. Yang, T. Hopf, S. M. Haerne, C. I. Pakes, S. Prawer, M. Mitic, E. Gauja, S. E. Andresen, F. E. Hudson, A. S. Dzurak, R. G. Clark, *Appl. Phys. Lett.* **2005**, *86*, 202101.

[41] W. Schnitzler, N. M. Linke, R. Fickler, J. Meijer, F. Schmidt-Kaler, K. Singer, *Phys. Rev. Lett.* **2009**, *102*, 070501.

[42] C. Sahin, P. Geppert, A. Müllers, H. Ott, *New J. Phys.* **2017**, *19*, 123005.

[43] P. Räcke, D. Spemann, J. W. Gerlach, B. Rauschenbach, J. Meijer, *Sci. Rep.* **2018**, *8*, 9781.

[44] P. Räcke, R. Staacke, J. W. Gerlach, J. Meijer, D. Spemann, *J. Phys. D: Appl. Phys.* **2019**, *52*, 305103.

[45] J. Meijer, B. Burchard, M. Dohman, C. Wittmann, T. Gaebel, I. Popa, F. Jelezko, J. Wrachtrup, *Appl. Phys. Lett.* **2005**, *87*, 261909.

[46] O. Lehtinen, B. Naydenov, P. Börner, K. Melentjevic, C. Müller, L. P. McGuinness, S. Pezzagna, J. Meijer, U. Kaiser, F. Jelezko, *Phys. Rev. B* **2016**, *93*, 035202.

[47] T. Lühmann, N. Raatz, R. John, M. Lesik, J. Rödiger, M. Portail, D. Wildanger, F. Kleißler, K. Nordlund, A. Zaitsev, J.-F. Roch, A. Tallaire, J. Meijer, S. Pezzagna, *J. Phys. D: Appl. Phys.* **2018**, *51*, 483002.

[48] X. J. Hu, Y. B. Dai, R. B. Li, H. S. Shen, X. C. He, *Solid State Commun.* **2002**, *122*, 45.

[49] M. Hauf, B. Grotz, B. Naydenov, M. Dankerl, S. Pezzagna, J. Meijer, F. Jelezko, J. Wrachtrup, M. Stutzmann, F. Reinhard, J. A. Garrido, *Phys. Rev. B* **2011**, *83*, 081304(R).

[50] F. Fávaro de Oliveira, D. Antonov, Y. Wang, P. Neumann, S. A. Momenzadeh, T. Häußermann, A. Pasquarelli, A. Denisenko, J. Wrachtrup, *Nat. Commun.* **2017**, *8*, 15409.

[51] T. Yamamoto, T. Umeda, K. Watanabe, S. Onoda, M. L. Markham, D. J. Twitchen, B. Naydenov, L. P. McGuinness, T. Teraji, S. Koizumi, F. Dolde, H. Fedder, J. Honert, J. Wrachtrup, T. Ohshima, F. Jelezko, J. Isoya, *Phys. Rev. B* **2013**, *88*, 075206.

[52] J. M. Smith, S. A. Meynell, A. C. Bleszynski Jayich, J. Meijer, *Nanophotonics* **2019**, *8*, 1889.

[53] A. M. Zaitsev, *Optical Properties of Diamond*, Springer, Berlin **2001**.

[54] B. Naydenov, V. Richter, J. Beck, M. Steiner, P. Neumann, G. Balasubramanian, J. Achard, F. Jelezko, J. Wrachtrup, R. Kalish, *Appl. Phys. Lett.* **2010**, *96*, 163108.

[55] S. Onoda, K. Tatsumi, M. Haruyama, T. Teraji, J. Isoya, W. Kada, T. Ohshima, O. Hanaizumi, *Phys. Status Solidi A* **2017**, *214*, 1700160.

[56] J. P. Goss, P. R. Briddon, M. J. Rayson, S. J. Sque, R. Jones, *Phys. Rev. B* **2005**, *72*, 035214.

[57] G. Thiering, A. Gali, *Phys. Rev. X* **2018**, *8*, 021063.

[58] C. Bradac, W. Gao, J. Forneris, M. E. Trusheim, I. Aharonovich, *Nat. Commun.* **2019**, *10*, 5625.

[59] J. N. Becker, C. Becher, *Phys. Status Solidi A* **2017**, *214*, 1700586.

[60] T. Schröder, M. E. Trusheim, M. Walsh, L. Li, J. Zheng, M. Schukraft, A. Sipahigil, R. E. Evans, D. D. Sukachev, C. T. Nguyen, J. L. Pacheco, R. M. Camacho, E. S. Bielejec, M. D. Lukin, D. Englund, *Nat. Commun.* **2016**, *8*, 15376.

[61] R. E. Evans, A. Sipahigil, D. D. Sukachev, A. S. Zibrov, M. D. Lukin, *Phys. Rev. Appl.* **2016**, *5*, 044010.

[62] S. Tamura, G. Koike, A. Komatsubara, T. Teraji, S. Onoda, L. P. McGuinness, L. Rogers, B. Naydenov, E. Wu, L. Yan, F. Jelezko, T. Ohshima, J. Isoya, T. Shinada, T. Tanii, *Appl. Phys. Express* **2014**, *7*, 115201.

[63] T. Iwasaki, F. Ishibashi, Y. Miyamoto, Y. Doi, S. Kobayashi, T. Miyazaki, K. Tahara, K. D. Jahnke, L. J. Rogers, B. Naydenov, F. Jelezko, S. Yamasaki, S. Nagamachi, T. Inubushi, N. Mizuochi, M. Hatano, *Sci. Rep.* **2015**, *5*, 12882.

[64] Y. Zhou, Z. Mu, G. Adamo, S. Bauerdick, A. Rudzinski, I. Aharonovich, W.-B. Gao, *New J. Phys.* **2018**, *20*, 125004.

[65] T. Iwasaki, Y. Miyamoto, T. Taniguchi, P. Siyushev, M. H. Metsch, F. Jelezko, M. Hatano, *Phys. Rev. Lett.* **2017**, *119*, 253601.

[66] S. Ditalia Tchernij, T. Herzig, J. Forneris, J. Küpper, S. Pezzagna, P. Traina, E. Moreva, I. P. Degiovanni, G. Brida, N. Skukan, M. Genovese, M. Jakšić, J. Meijer, P. Olivero, *ACS Photonics* **2017**, *4*, 2580.

[67] J. Görlitz, D. Herrmann, G. Thiering, P. Fuchs, M. Gandil, T. Iwasaki, T. Taniguchi, M. Kieschnick, J. Meijer, M. Hatano, A. Gali, C. Becher, *New J. Phys.* **2020**, *22*, 013048.

[68] S. Ditalia Tchernij, T. Lühmann, T. Herzig, J. Küpper, A. Damin, S. Santonocito, M. Signorile, P. Traina, E. Moreva, F. Celegato, S. Pezzagna, I. P. Degiovanni, P. Olivero, M. Jakšić, J. Meijer, P. M. Genovese, J. Forneris, *ACS Photonics* **2018**, *5*, 4864.

[69] S. Y. Lee, M. Widmann, T. Rendler, M. W. Doherty, T. M. Babinec, S. Yang, M. Eyer, P. Siyushev, B. J. M. Hausmann, M. Loncar, Z. Bodrog, A. Gali, N. B. Manson, H. Fedder, J. Wrachtrup, *Nat. Nanotechnol.* **2013**, *8*, 487.

[70] R. John, J. Lehnert, M. Mensing, D. Spemann, S. Pezzagna, J. Meijer, *New J. Phys.* **2017**, *19*, 053008.

[71] P. Balasubramanian, M. H. Metsch, P. Reddy, L. J. Rogers, N. B. Manson, M. W. Doherty, F. Jelezko, *Nanophotonics* **2019**, *8*, 11.

[72] J. C. Arnault, S. Saada, C. Mer-Calfati, F. Jomard, N. Habka, J. Barjon, J. Chevallier, *Phys. Lett. A* **2010**, *374*, 3254.

[73] J. Barjon, N. Habka, J. Chevallier, F. Jomard, E. Chikoidze, C. Mer-Calfati, J. C. Arnault, P. Bergonzo, A. Kumar, J. Pernod, F. Omnès, *Phys. Chem. Chem. Phys.* **2011**, *13*, 11511.

[74] A. Stacey, T. J. Karle, L. P. McGuinness, B. C. Gibson, K. Ganesan, S. Tomljenovic-Hanic, A. D. Greentree, A. Hoffman, R. G. Beausoleil, S. Prawer, *Appl. Phys. Lett.* **2012**, *100*, 071902.

[75] C. Saguy, C. Cytermann, B. Fitzgeer, Y. Avigal, N. Moriya, R. Kalish, B. Mathieu, A. Deneuville, *Diamond Relat. Mater.* **2003**, *12*, 623.

[76] C. B. Hartland, *Ph.D. Thesis*, University of Warwick, **2014**.

[77] S. Chakravarthi, C. Moore, A. Opsvig, C. Pederson, E. Hunt, A. Ivanov, I. Christen, S. Dunham, K.-M. C. Fu, *Phys. Rev. Mater.* **2020**, *4*, 023402.

[78] S. T. Alsid, J. F. Barry, L. M. Pham, J. M. Schloss, M. F. O'Keeffe, P. Cappellaro, D. A. Braje, *Phys. Rev. Appl.* **2019**, *12*, 044003.

[79] J. M. Baker, D. C. Hunt, M. E. Newton, D. J. Twitchen, *Radiat. Eff. Defects Solids* **1999**, *149*, 233.

[80] M. A. Lea-Wilson, J. N. Lomer, J. A. van Wyk, *Philos. Mag. B* **1995**, *72*, 81.

[81] S. Dannefaer, K. Iakoubovskii, *J. Phys.: Condens. Matter* **2008**, *20*, 235225.

[82] G. Davies, A. T. Collins, *Diamond Relat. Mater.* **1993**, *2*, 80.

[83] J. Bernhole, A. Antonelli, T. M. Del Sole, *Phys. Rev. Lett.* **1988**, *61*, 2689.

[84] S. J. Breuer, P. R. Briddon, *Phys. Rev. B* **1995**, *51*, 6984.

[85] A. Mainwood, *Phys. Status Solidi A* **1999**, *172*, 25.

[86] K. Iakoubivskii, I. Kiflawi, K. Johnston, A. Collins, G. Davies, A. Stesmans, *Phys. B: Condens. Matter* **2003**, *340*, 67.

[87] K. Iakoubivskii, S. Dannefaer, A. Stesmans, *Phys. Rev. B* **2005**, *71*, 233201.

[88] L. Allers, A. T. Collins, J. Hiscock, *Diamond Relat. Mater.* **1998**, *7*, 228.

[89] L. Dei Cas, S. Zeldin, N. Nunn, M. Torelli, A. I. Shames, A. M. Zaitsev, O. Shenderova, *Adv. Funct. Mater.* **2019**, *29*, 1808362.

[90] A. T. Collins, *J. Phys. C: Solid State Phys.* **1980**, *13*, 2641.

[91] A. Mainwood, *Phys. Rev. B* **1994**, *49*, 7934.

[92] H. Kato, T. Makino, S. Yamakasi, H. Okushi, *J. Phys. D: Appl. Phys.* **2007**, *40*, 6189.

[93] J. P. Goss, R. Jones, M. I. Heggie, C. P. Ewels, P. R. Briddon, S. Öberg, *Phys. Rev. B* **2002**, *65*, 115207.

[94] P. Deák, B. Aradi, M. Kaviani, T. Frauenheim, A. Gali, *Phys. Rev. B* **2014**, *89*, 075203.

[95] M. Lesik, N. Raatz, A. Tallaire, P. Spinicelli, R. John, J. Achard, A. Gicquel, V. Jacques, J.-F. Roch, J. Meijer, S. Pezzagna, *Phys. Status Solidi A* **2016**, *213*, 2594.

[96] A. M. Edmonds, U. F. S. D'Haenens-Johansson, R. J. Cruddace, M. E. Newton, K.-M. C. Fu, C. Santori, R. G. Beausoleil, D. J. Twitchen, M. L. Markham, *Phys. Rev. B* **2012**, *86*, 035201.

[97] M. K. Atumi, J. P. Goss, P. R. Briddon, M. J. Rayson, *Phys. Rev. B* **2013**, *88*, 245301.

[98] B. C. Rose, D. Huang, Z.-H. Zhang, P. Stevenson, A. M. Tyryshkin, S. Sangtawesin, S. Srinivasan, L. Loudin, M. L. Markham, A. M. Edmonds, D. J. Twitchen. S. A. Lyon, N. P. de Leon, *Science* **2018**, *361*, 60.

[99] M.-A. Pinault-Thaury, B. Berini, I. Stenger, E. Chikoidze, A. Lusson, F. Jomard, J. Chevallier, J. Barjon, *Appl. Phys. Lett.* **2012**, *100*, 192109.

[100] R. Kalish, *Diamond Relat. Mater.* **2001**, 10, 1749.

[101] S. Koizumi, K. Watanabe, M. Hasegawa, H. Kanda, *Science* **2001**, *292*, 1899.

[102] R. G. Farrer, *Solid State Commun.* **1969**, 7, 685.

[103] A. T. Collins, *J. Phys.:Condens. Matter* **2002**, *14*, 3743.

[104] N. B. Manson, M. Hedges, M. S. J. Barson, R. Ahlefeldt, M. W. Doherty, H. Abe, T. Ohshima, M. J. Sellars, *New J. Phys.* **2018**, *20*, 113037.

[105] V. A. Chernyshev, J. Meijer, D. Grambole, F. Herrmann, Ü. Dagkaldiran, A. D. Wieck, *Diamond Relat. Mater.* **2008**, *17*, 1933.

[106] J. M. Baker, J. A. van Wyk, J. P. Goss, P. R. Briddon, *Phys. Rev. B* **2008**, *78*, 235203.

[107] D. Saada, J. Adler, R. Kalish, *Appl. Phys. Lett.* **2000**, *77*, 878.

[108] E. B. Lombardi, A. Mainwood, K. Osuch, *Phys. Rev. B* **2004**, *70*, 205201.

[109] K. Nakazawa, M. Tachiki, H. Kawarada, A. Kawamura, K. Horiuchi, T. Ishikura, *Appl. Phys. Lett.* **2003**, *82*, 2074.

[110] J. F. Prins, *Phys. Rev. B* **2000**, *61*, 7191.

[111] K. Groot-Berning, N. Raatz, I. Dobrinets, M. Lesik, P. Spinicelli, A. Tallaire, J. Achard, V. Jacques, J.-F. Roch, A. M. Zaitsev, J. Meijer, S. Pezzagna, *Phys. Status Solidi A* **2014**, *211*, 2268.

[112] N. Aslam, G. Waldherr, P. Neumann, F. Jelezko, J. Wrachtrup, *New J. Phys.* **2013**, *15*, 013064.

[113] Y. Doi, T. Fukui, H. Kato, T. Makino, S. Yamasaki, T. Tashima, H. Morishita, S. Miwa, F. Jelezko, Y. Suzuki, N. Mizuochi, *Phys. Rev. B* **2016**, *93*, 081203(R).

[114] T. Mittiga, S. Hsieh, C. Zu, B. Kobrin, F. Machado, P. Bhattacharyya, N. Z. Rui, A. Jarmola, S. Choi, D. Budker, N. Y. Yao, *Phys. Rev. Lett.* **2018**, *121*, 246402.

[115] G. M. Müller, M. Oestreich, M. Römer, J. Hübner, *Phys. E* **2010**, *43*, 569.

[116] J. F. Barry, J. M. Schloss, E. Bauch, C. A. Hart, L. M. Pham, R. L. Walsworth, *Rev. Modern Phys.* **2020**, *92*, 015004.

[117] R. Kalish, C. Uzan-Saguy, R. Walker, S. Prawer, *J. Appl. Phys.* **2003**, *94*, 3923.

[118] M. Hasegawa, M. Ogura, D. Takeuchi, S. Yamanaka, H. Watanabe, S. Ri, N. Kobayashi, H. Okushi, T. Sekiguchi, *Solid State Phenomena* **2001**, *78*, 171.

[119] T. Vogel, J. Meijer, A. Zaitsev, *Diamond Relat. Mater.* **2004**, *13*, 1822.

[120] T. Lühmann, J. Küpper, S. Dietel, R. Staacke, J. Meijer, S. Pezzagna, *ACS Photonics* **2020**, *7*, 3376.

[121] H. Hofsäss, M. Dalmer, M. Restle, C. Ronning, *J. Appl. Phys.* **1997**, *81*, 2566.

[122] R. Kalish, C. Uzan-Saguy, B. Philosoph, V. Richter, J. P. Lagrange, E. Gheeraert, A. Deneuville, A. T. Collins, *Diamond Relat. Mater.* **1997**, *6*, 516.

[123] B. Naydenov, F. Reinhard, A. Lämmle, V. Richter, R. Kalish, U. F. S. D'Haenens-Johansson, M. Newton, F. Jelezko, J. Wrachtrup, *Appl. Phys. Lett.* **2010**, *97*, 242511.

[124] S. Salustro, F. S. Gentile, A. Erba, P. Carbonniére, K. E. El-Kelany, R. Dovesi, *Carbon* **2018**, *132*, 210.

[125] M. N. R. Ashfold, J. P. Goss, B. L. Green, P. W. May, M. E. Newton, C. V. Peaker, *Chem. Rev.* **2020**, *120*, 5745.

Tobias Lühmann is a Ph.D. candidate in the group Applied Quantum Systems at the Universität Leipzig, Germany. He works on the engineering of defect formation using doping and on the annealing behavior of damage in diamond. He aims at the deterministic creation of various color centers in diamond, and at the control of their environment by studying their optical and spin properties.

Jan Meijer is leading the group Applied Quantum Systems at the Universität Leipzig, Germany, since 2013. He received his Ph.D. degree in physics in 1997 from the University Münster. From 1997 to 2004 he was a senior scientist at the Ruhr-Universität Bochum and between 2004 and 2012 was the managing director of the Central Laboratories of Ion Beams and Radionuclides. His research topics cover deterministic ion implantation, assembling of single ions with high spatial resolution, and applied quantum systems for sensing and computing.

Sébastien Pezzagna is a senior research scientist in the group Applied Quantum Systems at the Universität Leipzig, Germany. He received his Ph.D. degree in physics in 2005 from the Université de Nice (France) with research topics on group III nitrides and nonlinear optics. From 2007 to 2013, he was a research fellow at the Ruhr-Universität Bochum. He developed high-resolution ion implantation techniques, especially for color centers in diamond. In 2013, he joined the Universität Leipzig and his main research interests are engineering, spectroscopy, and new applications of single defects in the solid state.